

The Nanoscience Revolution: Merging of Colloid Science, Catalysis and Nanoelectronics

Gabor A. Somorjai · Feng Tao · Jeong Young Park

Published online: 7 February 2008
© Springer Science+Business Media, LLC 2008

Abstract The incorporation of nanosciences into catalysis studies has become the most powerful approach to understanding reaction mechanisms of industrial catalysts and designing new-generation catalysts with high selectivity. Nanoparticle catalysts were synthesized via controlled colloid chemistry routes. Nanostructured catalysts such as nanodots and nanowires were fabricated with nanolithography techniques. Catalytic selectivity is dominated by several complex factors including the interface between active catalyst phase and oxide support, particle size and surface structure, and selective blocking of surface sites, etc. The advantage of incorporating nanosciences into the studies of catalytic selectivity is the capability of separating these complex factors and studying them one by one in different catalyst systems. The role of oxide–metal interfaces in catalytic reactions was investigated by detection of continuous hot electron flow in catalytic nanodiodes fabricated with shadow mask deposition technique. We found that the generation mechanism of hot electrons detected in Pt/TiO₂ nanodiode is closely correlated with the turnover rate under CO oxidation. The correlation suggests the possibility of promoting catalytic selectivity by precisely controlling hot electron flow at the oxide–metal interface. Catalytic activity of 1.7–7.2 nm monodispersed Pt nanoparticles exhibits particle size dependence, demonstrating the enhancement of catalytic selectivity via controlling the size of catalyst. Pt–Au alloys with different

Au coverage grown on Pt(111) single crystal surface have different catalytic selectivity for four conversion channels of *n*-hexane, showing that selective blocking of catalytic sites is an approach to tuning catalytic selectivity. In addition, presence and absence of excess hydrogen lead to different catalytic selectivity for isomerization and dehydrocyclization of *n*-hexane on Pt(111) single crystal surface, suggesting that modification of reactive intermediates by the presence of coadsorbed hydrogen is one approach to shaping catalytic selectivity. Several challenges such as imaging the mobility of adsorbed molecules during catalytic reactions by high pressure STM and removing polymeric capping agents from metal nanoparticles remain.

Keywords Nanoscience · Nanotechnology · Colloid science · Catalysis · High pressure · Scanning tunnelling microscopy

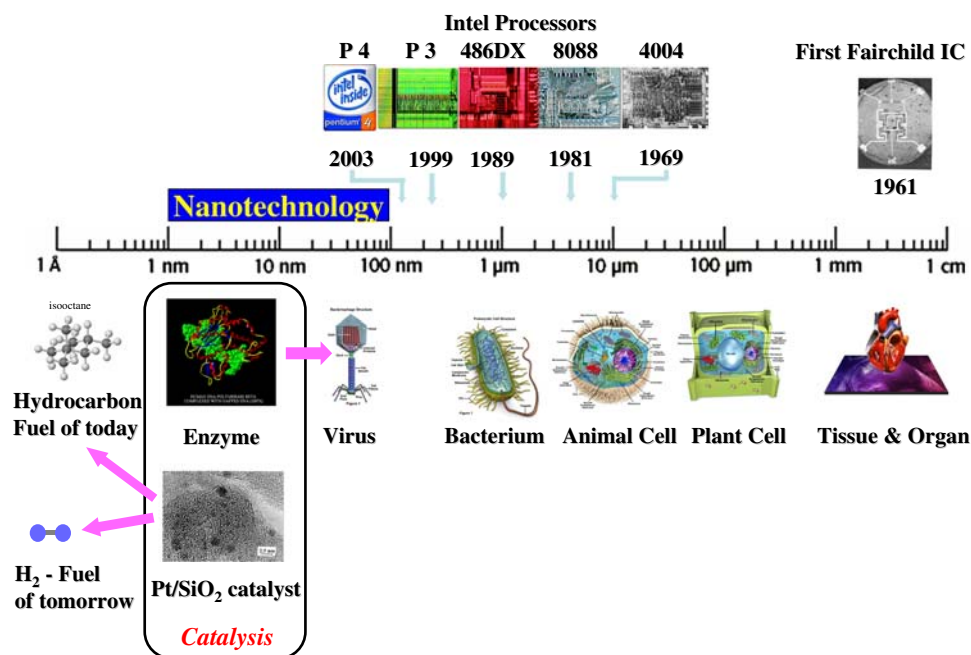
1 Introduction

Metal-containing catalysts, metallic heterogeneous and homogeneous catalyst, and enzyme are nanoparticles in the 1–10 nm range. Figure 1 illustrates the scale effects of catalytic, biological and microelectronic systems shaped by nanosciences and nanotechnology. Nanoscale heterogeneous catalysts are usually deposited in high surface area oxide support to optimize their surface area and therefore their turnover rates and also optimize their thermal and chemical stability when used in the presence of vapor phase reactants and products at 400–800 K range. Enzyme catalysts operate in solution, mostly in water at 300 K while homogeneous catalysts function in mostly organic solvent in the 300–500 K range.

G. A. Somorjai · F. Tao · J. Y. Park
Materials Science Division, Lawrence Berkeley National
Laboratory, Berkeley, CA 94720, USA

G. A. Somorjai (✉) · F. Tao · J. Y. Park
Department of Chemistry, University of California, Berkeley,
CA 94720, USA
e-mail: somorjai@socrates.berkeley.edu

Fig. 1 Important catalytic, biological and microelectronic systems in nanometer regime



The field of metal heterogeneous catalyst developed rapidly by use of model catalyst, first single crystal surface [1], then monodispersed nanoclusters deposited on oxide surface by lithography techniques [2–7] or by colloid chemistry [8–12]. While single crystal could reproduce many of the elementary steps of industrial catalytic reactions where there is only one product (quinoline synthesis, carbon monoxide oxidation, and ethylene hydrogenation), for multi-path reaction with several reaction products the selectivity depends on ingredients such as the oxide–metal interface and the presence of a second metal that selectively blocks surface sites. Our model metal catalyst nanoparticles deposited on oxide surfaces could reproduce most ingredients of reaction selectivity that the single crystals could not.

In this paper we described the fabrication of platinum nanoparticles using lithography and the synthesis of catalytic nanoparticles by colloid techniques in solution. Monodispersed platinum nanoparticles could be deposited on a planar support such as a silicon wafer in two dimension (2D) using Langmuir-Blodgett techniques or encapsulated in a mesoporous high surface area oxide to produce a three-dimensional (3D) catalyst system.

By using metal nanoparticle model system we demonstrated the importance of particle size in catalytic selectivity. The unique chemical activity of oxide–metal interfaces is shown to be due in part to electron flow from the metal to the oxide through a Schottky barrier at the interface. We constructed a catalytic nanodiode to investigate the electron flow during the catalytic reaction and found that electron flow and reaction turnover rate do correlate.

We hope to show in this paper that the size of nanoscience of catalysis leads to the determination of molecular ingredients that control reaction selectivity. We believe it will be possible to develop “green catalysts” which produce only the desired product molecules without byproducts.

2 Synthesis of 2-D and 3-D Nanocatalysts

The approaches we used for fabricating 2-D or 3-D nanocatalysts with precise control at molecular and even atomic levels are nanolithography fabrication and colloid synthesis. Using these nanofabrication techniques, we synthesized monodispersed nanocatalysts with controlled size, oxide–metal interface, distribution of catalytic metal particles in support matrix, and even shape.

2.1 Formation of 2-D Nanocatalyst by Nanolithography

Lithography-based nanocatalyst fabrication is one of the main techniques we developed for the production of high-technology catalysts. It has the advantage of precise control of particle size and inter-particle distance. The formed 2-D array of nanocatalysts is highly monodispersed. It can controllably form a oxide–metal interface which offers opportunity for studying the role of the interface between catalytically active phase and support in catalytic reactions. Moreover, a fabricated 2-D array of nanodots or nanowires can be easily cleaned and crystallized for catalyst studies.

Most importantly, the nanolithography routes exemplified in this section are applicable to the fabrication of any other 2-D nanocatalysts on different substrates.

The simplest route is electron beam lithography (EBL) [5, 6], which utilizes high-resolution pattern writing and an electron sensitive resist/etching. It can fabricate nanoparticles with a size of ~ 10 nm. However, it is limited by low throughput and high cost. A new method developed by us is called size reduction lithography (SRL) [7]. Figure 2 schematically presents the route of one cycle. Several repetitions of this protocol can reduce the mold from 0.6 μm poly-silicon to ~ 7 nm silicon nanowire. The nanowire pattern is transferred into poly methylmethacrylate (PMMA) under high pressure and high temperature by using nano imprint lithography (NIL). Then, a thermal oxide layer formed by oxygen-plasma etching upon residual PMMA is removed. Thus, a nanoscale mold is fabricated. Figure 3 presents the multiplication of pattern density by SRL. Pt atoms can be deposited by electron beam evaporation to form Pt nanowires [13]. Thermal treatment in vacuum, hydrogen or oxygen crystallized the Pt nanowires [14, 15]. The major contaminant, carbon from PMMA can be removed by thermal oxidation under low pressure (1×10^{-6} Torr) of NO_2 at 573 K. The adsorbed oxygen after the step of carbon removal can be removed by converting into CO_2 with CO.

Another new method we developed for the fabrication of catalytic nanodots is called mold-to-mold cross imprint (MTMCI) [4]. This technique is capable of producing high areal density nanodots of any metal on any surface. It includes three main steps. First, a silicon wire mold is fabricated by spacer lithography. Details of the fabrication process were described elsewhere [16]. Second, a mold-to-mold cross imprint (MTMCI) technique is used to convert

the silicon spacer nanowires into silicon nanopillars. The principle of the second step is to pattern a silicon spacer nanowire mold with another nanowire mold by imprinting one mold placed perpendicularly onto the other. Figure 4a shows the protocol for the fabrication of silicon nanodot model in the MTMCI techniques. In the second step, an array of silicon nanopillars is fabricated at the intersection of the silicon and chromium nanowires by etching the silicon. The formed silicon nanopillars have a size of $15 \times 30 \times 250$ nm. Figure 4b is an array of silicon nanopillars which acts as the final mold for the fabrication of 2-D catalytic nanodots on substrate. The third step is the imprinting of Pt nanodots (Fig. 5). The silicon nanopillar mold is imprinted into a PMMA layer on silicon oxide layers naturally formed on commercially available silicon wafer. A thin layer of Cr is deposited as a hard mask for PMMA mold via angled evaporation. Then, Pt atoms are deposited into the uncovered nanowell, forming Pt nanodots with dimensions of $15 \times 30 \times 5$ nm. Figure 4c is an array of Pt nanodots on silicon oxide upon residual PMMA is removed. Compared to the cleaning and crystallization of Pt nanowires fabricated through SRL, similar cleaning routes [14, 15] are used for cleaning and crystallization of the Pt nanodots.

2.2 Colloid Chemistry Controlled Synthesis of 2-D and 3-D Nanocatalysts

Controlled colloid chemistry reaction is one of the main techniques for the syntheses of nanoparticles of metal, semiconductor, and magnetic materials. Figure 6 illustrates this technique. Synthesis of 3-D nanocatalysts through colloid chemistry has several advantages. The size of

Fig. 2 One cycle of the protocol used to reduce the size of mold in size reduction lithography

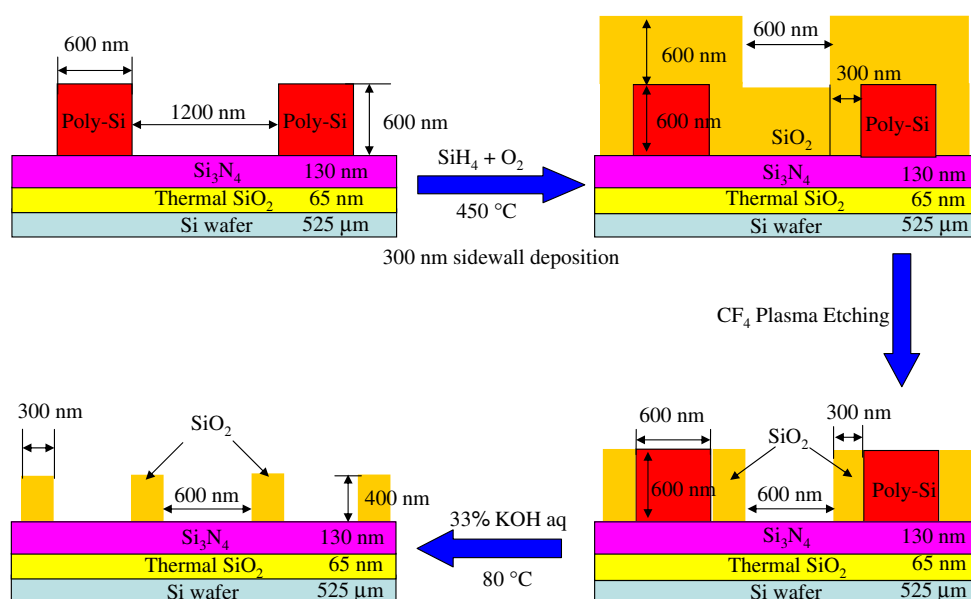
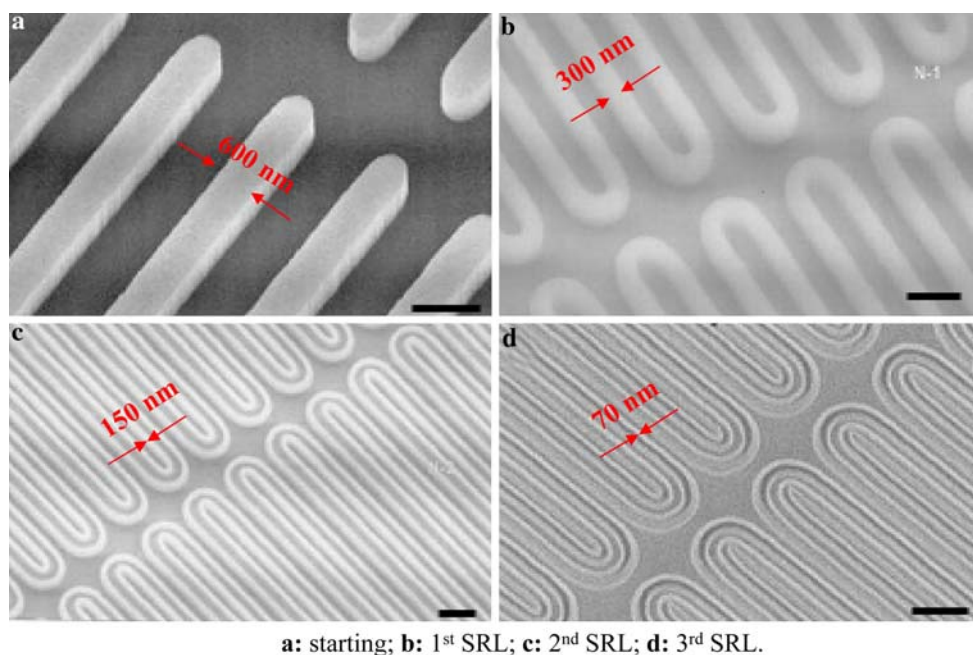


Fig. 3 Multiplication of pattern density by size reduction lithography. (a) after patterning sacrificial poly-Si layer, (b) after SiO₂ deposition, SiO₂ spacer etch by CF₄ plasma, and removal of sacrificial poly-Si by KOH, (c) after poly-Si deposition, poly-Si spacer etch by Cl₂ and HBr, and removal of SiO₂ by HF, and (d) after SiO₂ deposition, SiO₂ spacer etch by CF₄ plasma, and removal of sacrificial poly-Si by KOH. Upon three time size reduction lithography, 8 ($=2^3$) lines with line width of 70 nm and interline spacing of 80 nm were generated after 3 fold reduction lithography. The scale bars in all images are 1 μm



a: starting; b: 1st SRL; c: 2nd SRL; d: 3rd SRL.

Fig. 4 (a) Scheme of mold-to-mold cross imprint (MTMCI) to fabricate a nanopillar mold. (b) SEM of a nanopillar mold (each nanopillar: 15 × 30 × 250 nm). (c) A homogenous array of Pt nanodots (each nanodot: 15 × 30 × 5 nm) made by MTMCI

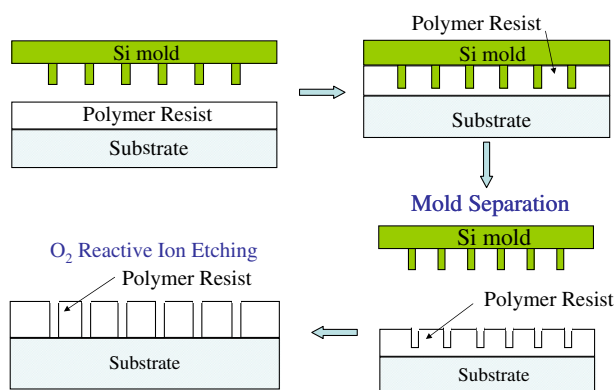
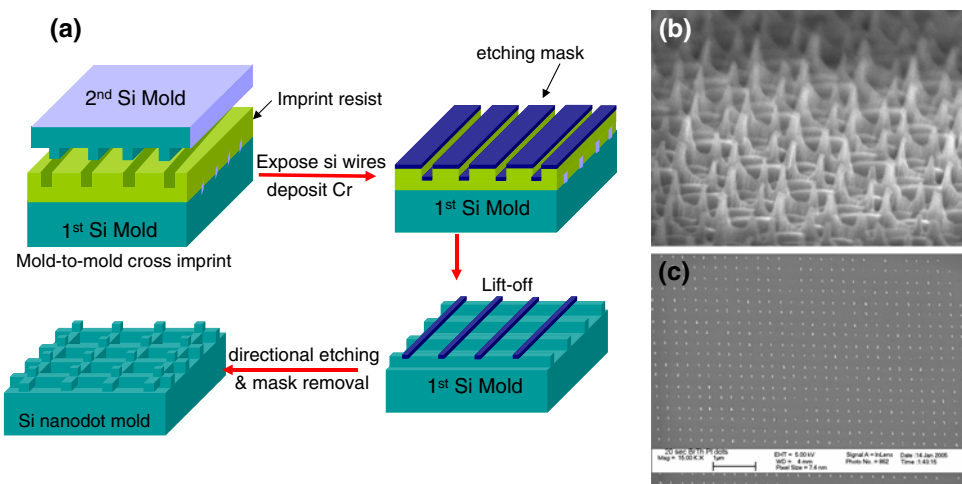


Fig. 5 Scheme of nanoimprint lithography

nanoparticles can be precisely controlled in the range of 1–30 nm. The 3-D nanoparticles have metal surface area of 1 m²/g or greater. In addition, the colloid chemistry synthesis can control nanoparticle shape to some extent. Definitely, this synthesis has high throughput. The core reaction for the production of metal particles is the reduction of metallic salts in solution. Chemical reduction methods including alcohol reduction, hydrogen reduction, and sodium borohydride reduction were reported [17–19]. Capping agents such as polymers, dendrimers, block copolymer micelles, and surfactants are used for stabilizing nanoparticles and preventing it from aggregation. Figure 7 is an example of the reactions we used for the synthesis of Pt nanoparticles. This method can produce monodispersed

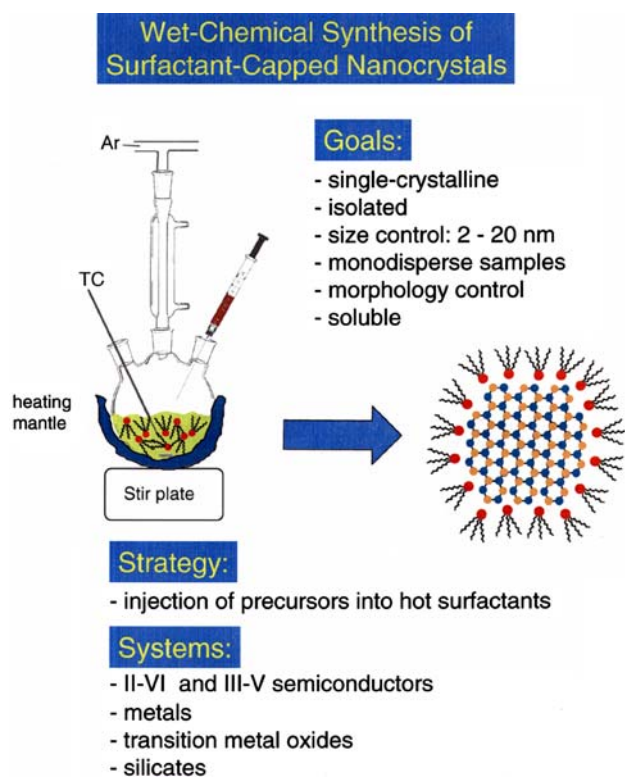


Fig. 6 Synthesis of nanoparticles with colloid chemistry

nanoparticles in the size range of 1.7–7.2 nm. As shown in Fig. 8, the synthesized Pt nanoparticles can be assembled into SBA-15 silica support via two different strategies. The first one is called capillary inclusion (CI) [12], in which SBA-15 is synthesized before inclusion. A low sonication can promote the inclusion of nanoparticles into SBA-15 in a water/ethanol solution of Pt nanoparticles and SBA-15 silica. Figure 9 shows two examples of Pt/SBA-15 catalysts assembled with capillary inclusion. The second strategy [11] is the *in-situ* hydrothermal synthesis of SBA-15 silica in a solution containing Pt nanoparticles and

Fig. 7 Reduction reaction for synthesis of Pt nanoparticles and transmission electron microscopy (TEM) images of the synthesized nanoparticles of 1.7–7.2 nm

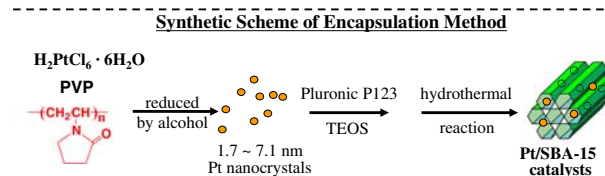
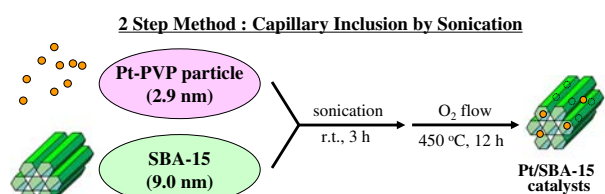
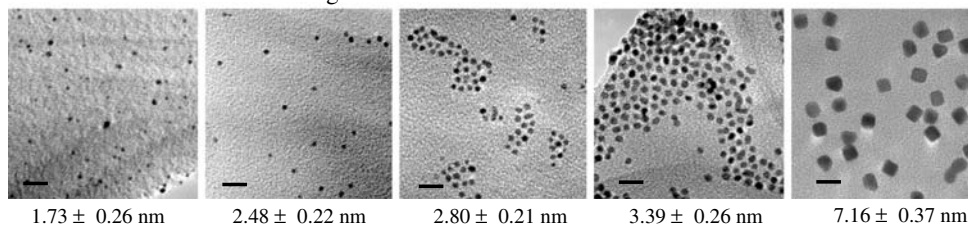
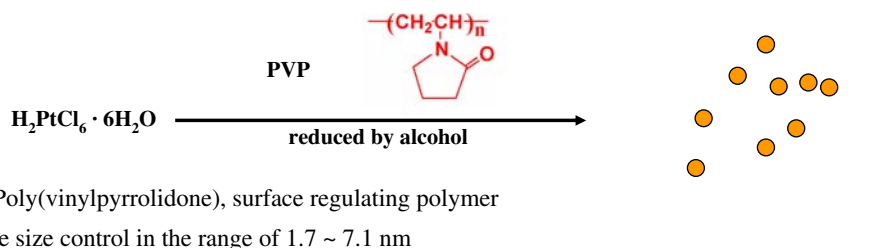


Fig. 8 Two strategies for the assembly of nanoparticles into SBA-15 support. Top panel: capillary inclusion. Bottom panel: encapsulation

starting materials for the synthesis of SBA-15. This route is called nanoparticle encapsulation (NE) which makes nanoparticles directly situate in the silica pore structure.

In addition, a 2-D assembly of the synthesized 3-D nanoparticles was developed as a new model catalyst. The Pt nanoparticles were immobilized onto the silicon oxide layer of Si wafer via a Langmuir–Blodgett experiment, forming a monolayer of monodispersed Pt nanoparticles. Figure 10 schematically shows the assembly of nanoparticles in a monolayer. This approach takes advantage of *both* the small and controllable size of nanoparticles synthesized with colloid chemistry route *and* the formation of oxide–metal interface between nanoparticles and substrate. The average inter-particle spacing can be tuned by varying surface pressure. Figure 11 is the dependence of surface area dispersed by one molar of nanoparticles on surface pressure.

The synthesized nanocatalyst needs to be activated. The activation is mainly the removal of the capping agent bound to nanoparticles. It is quite challenging. Generally, it is activated by thermal treatment in an inert atmosphere or oxygen followed by reduction to produce an active catalyst.

Fig. 9 TEM images of Pt/SBA-15 nanocatalysts synthesized via colloid chemistry and then assembled with capillary inclusion

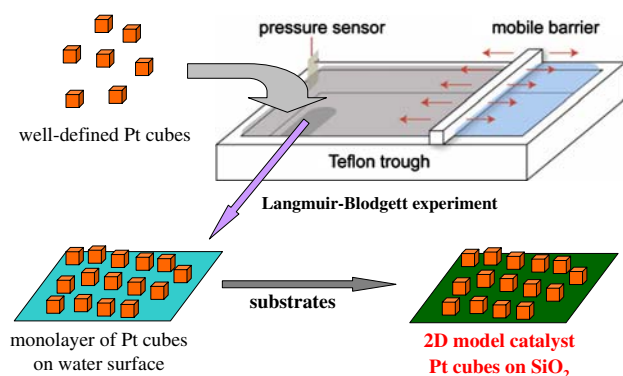
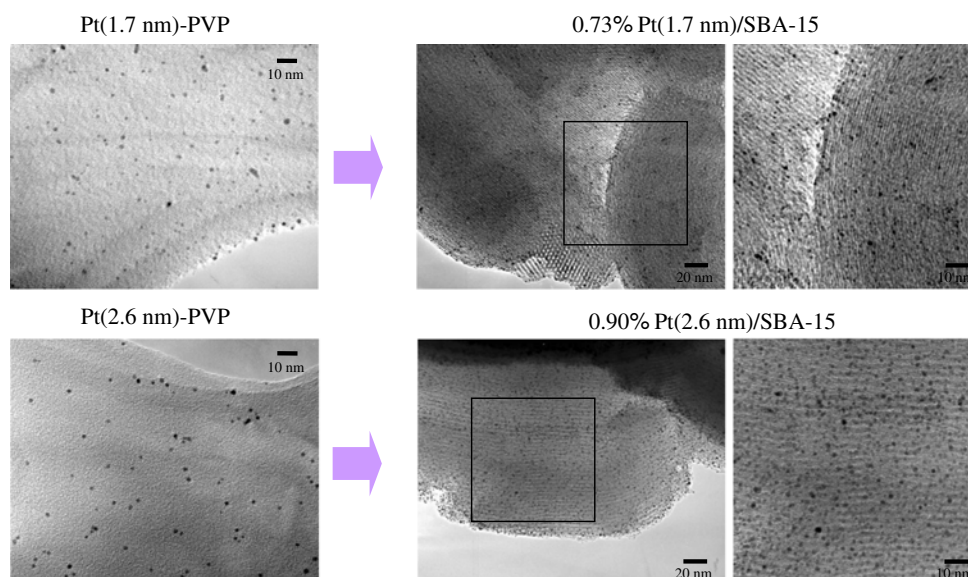


Fig. 10 Scheme for the formation Langmuir–Blodgett monolayer of 3-D Pt nanoparticles on silicon oxide

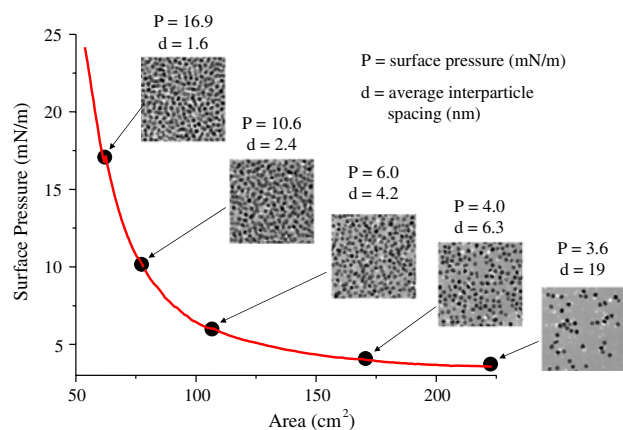


Fig. 11 The applied surface pressure as a function of surface area dispersed by one molar of Pt nanoparticles. Higher surface pressure corresponds to smaller inter-particle spacing

The temperature of thermal treatment is crucial. Too high a temperature results in severe agglomeration of the nanoparticles; too low a temperature leaves much carbon

contaminant blocking reactive sites of nanoparticles. We activated Pt/SBA-15 catalysts with O₂ at 623–723 K for 24–26 h followed by a reduction with H₂ [11, 12].

3 Characterization of Nanocatalyst Structure and Surface Area

Structure of 2-D nanocatalysts on solid substrate fabricated via various nanolithography routes was characterized by scanning electron microscopy (SEM). The shape of 3-D nanoparticles was identified by TEM. In addition, TEM was used for checking the distribution of Pt nanoparticles in SBA-15 since an efficient incorporation of Pt nanoparticles into SBA-15 is important for a high activity of these metal/mesoporous silica catalysts. Size of 3-D nanoparticles was measured by several techniques including TEM, X-ray diffraction (XRD), and chemisorption of H₂, O₂ or CO [11, 12]. The Pt nanoparticle sizes measured by the three techniques are nearly in agreement. However, particle size obtained by chemisorption of selective gases is the best measure of the catalytically relevant particle size. Adsorption of probe gases was used to normalize the measured reaction rates to the exposed surface area of nanoparticles [11, 12].

4 The Ingredients of Highly Selective Metal Catalysts

Selectivity, activity, and stability are the most important parameters of a catalyst. The design of a catalyst system producing only one desired product out of many other possible products (100% or near 100% selectivity) is one of the main goals of high-technology catalyst research. The

application of high-technology catalysts with 100% selectivity in industry is definitely a “green chemistry” process which eliminates the possibility of producing undesirable waste. For this purpose, our approach is to incorporate ingredients of selectivity into catalyst synthesis and catalysis study. The ingredients of catalytic selectivity revealed so far mainly include oxide–metal interface sites, metal particle size and surface structure, selective blocking of surface sites, and hydrogen pressure, though more ingredients could be uncovered in the future. These interacting ingredients are complex. Our approach was to isolate these ingredients and only study one of them in each different catalyst system. Thus, we used catalytic nanodiodes to understand the issue of oxide–metal interface sites, 2-D and 3-D Pt nanocatalysts to address the ingredient of metal particle size and surface structure, Pt/Au alloy catalyst systems to study selective site blocking, and catalytic conversion of *n*-hexane on Pt(111) to investigate the influence of hydrogen pressure on catalytic selectivity. Sum frequency generation, a surface-specific vibrational spectroscopy which can operate in a pressure range from ultra-high vacuum to atmosphere pressure [20], was used for the identification of reactive intermediates and products of catalytic reactions studied.

4.1 Oxide–Metal Interface

Over last 50 years, a number of heterogeneous catalytic studies showed that chemically inert oxides such as titania and silicon oxide deposited on catalytically active transition metal surfaces (Rh, Ni, Pt ...) largely enhanced catalytic activity and changed selectivity for metal catalysts [21–23]. For example, CO hydrogenation over a polycrystalline Rh foil deposited with a TiO₂ overlayer shows a threefold enhancement in activity for methanation and a higher selectivity toward olefins in contrast to bare Rh catalyst [21]. This effect was also investigated by Boffa and others [24] using rhodium deposited on a large number of oxides. They observed a remarkable 14-fold increase in turnover rates for CO₂ hydrogenation, especially in the presence of three different oxides, TiO_x, NbO_x, and TaO_x. The activity was at a maximum when the oxide–metal interface area was at a maximum, which occurred at about one-half of a monolayer of oxide coverage. These studies suggested that the oxide–metal interface plays an important role in catalytic reaction and is one ingredient of catalytic selectivity. However, understanding the role of oxide–metal interface in catalytic reaction is critically dependent on advanced surface probes. Until now no surface analytic technique has clearly addressed this issue. Recently, we developed catalytic metal/semiconductor Schottky nanodiodes and used them for studying the role of the interface

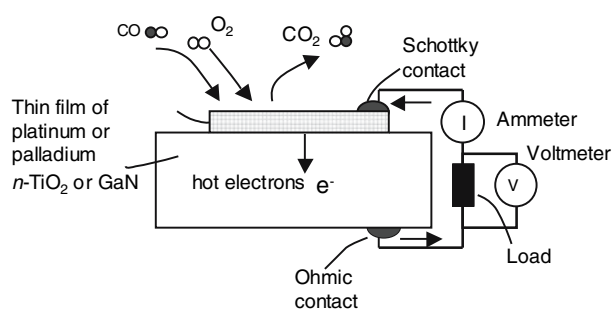


Fig. 12 Configuration of catalytic nanodiode using an exothermic catalytic reaction to generate hot electrons

between catalyst active phase and support in catalytic activity and selectivity [25]. Figure 12 shows the schematic of catalytic nanodiode. Briefly, if the metal particle or film is of the diameter or thickness of the electron mean free path (~ 10 nm) hot electrons can be collected as they are transported across the metal without collision. For an *n*-type Schottky diode, hot electrons are detected as a chemi-current if their excess energy is larger than the effective Schottky barrier. Two types of Schottky nanodiodes (Pt/TiO₂ and Pt/GaN) were fabricated with a shadow mask deposition technique, and used to generate steady state current under CO oxidation [26, 27]. The schemes of these devices are shown in Fig. 13. A detailed description of the fabrication of the two diodes can be found in literature [26, 27]. A reaction chamber with a volume of ~ 1 L with the electrical measurement was built to carry out gas reaction on the nanodiodes (Fig. 14).

Production and accumulation of CO₂ molecules was also measured during carbon monoxide oxidation by using gas chromatography. Figure 15 shows the chemi-current measured with three different diodes under 100 Torr of

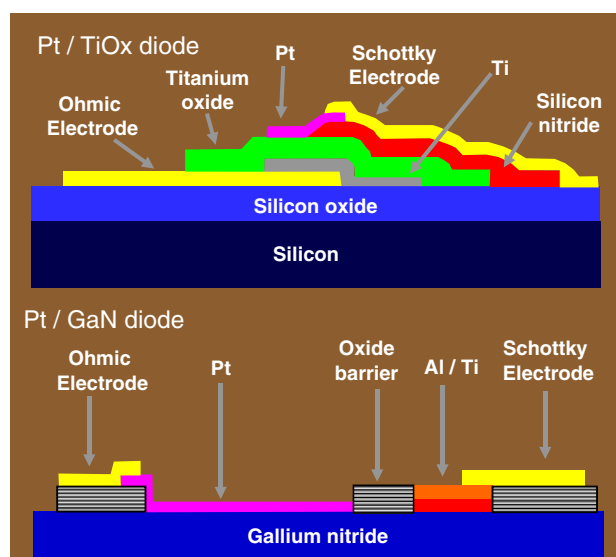


Fig. 13 Schemes of Pt/GaN and Pt/TiO₂ nanodiodes

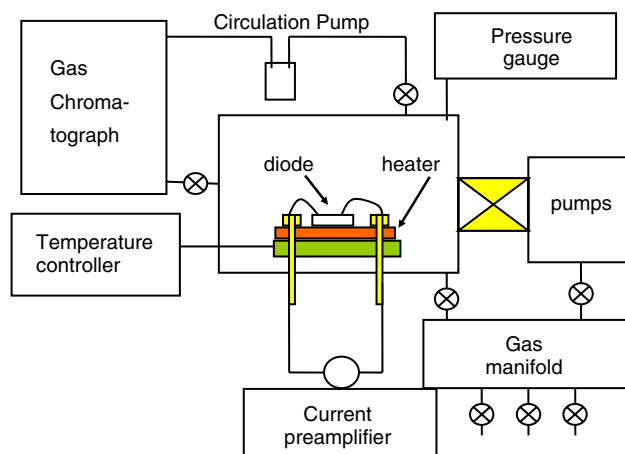


Fig. 14 Scheme of apparatus used for the catalytic studies and the detection of hot electron flow generation by catalytic oxidation of carbon monoxides on a Pt/GaN diode or a Pt/TiO₂ diode. A circulation pump was assembled for maintaining pressure of the reactant gas. A gas chromatography was connected to the chamber to detect product. The concentration of product was used to calculate turnover rate of catalytic reaction. The hot electron current between the two Au electrodes was measured with a current preamplifier during catalytic reaction (applied voltage = 0 V). The sample was heated by a ceramic heater and the temperature was measured with the thermocouple fixed between the back of the sample and heater

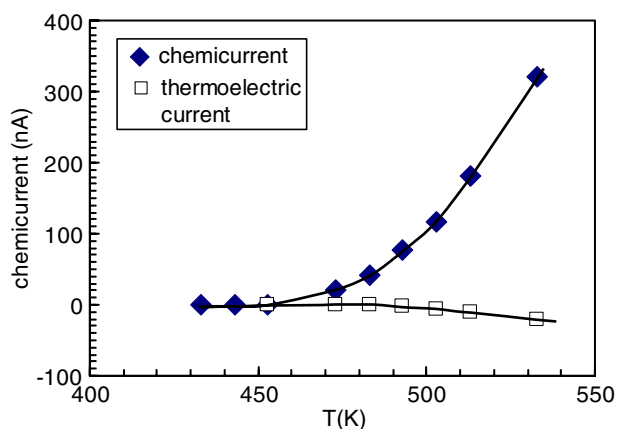


Fig. 15 Plot of chemicurrent detected under CO oxidation (100 Torr of O₂ and 40 Torr of CO) with Pt/TiO₂ diode as a function of the temperature. The thermoemetric current was measured as a function of temperature by heating the same diode in He (1 atm)

oxygen and 40 Torr of carbon monoxide as a function of the temperature. Each data point in the chemicurrent represents the average of 100 data points. With the increase of reaction temperature, thermoemetric current appeared as one component of the detected current. By heating the nanodiodes in He, we could measure the thermoemetric current alone. Because the thermoemetric current detected in Pt/TiO₂ diode is always in the opposite direction of the hot electron current generated from catalytic reaction, the effective hot electron current (also called chemicurrent) is

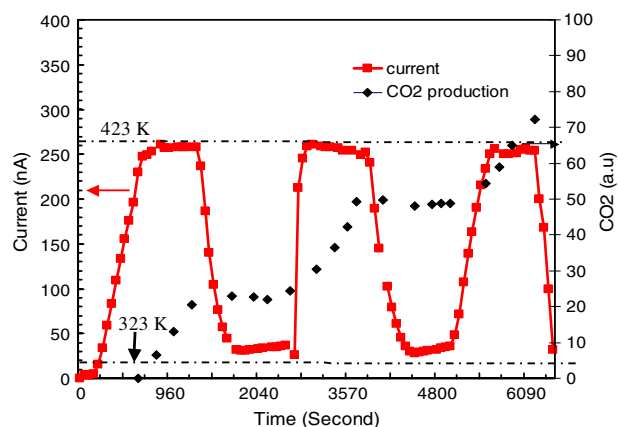


Fig. 16 Hot electron generation and CO₂ accumulation cycles between 423 K and 323 K. The reaction conditions are 100 Torr of O₂ and 40 Torr of CO. Hot electron generation was controlled by reaction rate of CO oxidation on the platinum thin film

the difference between the detected current during catalytic reaction and the thermoemetric current [28]. The measurement of chemicurrent in catalytic nanodiode clearly demonstrated that chemical energy of exothermic catalytic reaction was directly converted into hot electron flux transporting through oxide–metal interface.

Figure 16 shows that the chemicurrent detected in Pt/GaN diode as changing the reaction temperature [26]. It is further evidence confirming the generation of hot electron due to catalytic reaction. The alternative change of hot electron generation (red line) is consistent with the accumulation cycles of the produced CO₂ (black line). Notably, our detection of hot electron current from catalytic nanodiodes is consistent with the early argument given by Schwab [29, 30], Solymosi [31], and Langenbeck et al. [32]. They suggested the importance of electron flow at oxide–metal interfaces for several catalysis reactions including CO oxidation, SO₂ oxidation, formic acid decomposition, ethylene hydrogenation, cyclohexene hydrogenation and dehydrogenation, and ammonia synthesis [31, 33]. The importance of electron flow through the oxide–metal interface for catalytic reaction on metal surface was confirmed by the difference in turnover rate between ethylene hydrogenation on Pt nanoparticles upon CO poisoning [34] and that on Pt single crystal surface [35] upon CO poisoning. For ethylene hydrogenation catalyzed by Pt nanoparticles deposited on Al₂O₃ and SiO₂ surfaces, the turnover rate is proportional to the oxide–metal periphery area though the nanoparticles are poisoned, and there is no change in activation energy of ethylene hydrogenation upon CO poisoning. Compared to Pt nanoparticles on Al₂O₃ or SiO₂ upon CO poisoning, the turnover rate of ethylene hydrogenation on Pt single crystal upon CO poisoning is negligible and the activation energy is largely increased to 22 kcal/mol. In addition, the significant particle size

dependence of catalytic activity of gold nanoparticles grown on TiO₂ [36] further supports the importance of hot electron flow at oxide–metal interface for catalytic reactions. Overall, a general rule is that the turnover rate of reaction catalyzed by some metals is proportional to the interface area between oxide and the metal. The electric field generated at the oxide–metal interface due to hot electron flow is possibly a factor for the promotion of turnover rates.

The understanding of the role of oxide–metal interface in catalytic selectivity is still under investigation. As mentioned before the variation of catalytic selectivity for CO hydrogenation upon the deposition of oxides on metal catalysts clearly demonstrated the important role of oxide–metal interface in catalytic selectivity on metal surface [21–23]. Promising approaches to promoting catalytic selectivity related to oxide–metal interface are to vary the electric field strength formed by hot electron flow of catalytic reaction, to apply an external bias voltage to switch the flow direction of hot electrons, to use oxide layer or metal thin film with different thickness, or to tune the structure of interface layer.

4.2 The Influence of Metal Particle Size and Surface Structure on Catalytic Selectivity

Particle size is one of the most important factors dominating catalytic selectivity. The selectivity of catalytic hydrogenation and dehydrogenation on Pt nanoparticles exhibits significant size dependence. Figure 17 is the size dependence of catalytic selectivity for cyclohexene hydrogenation and dehydrogenation on Pt nanoparticles (blue line for hydrogenation into cyclohexane, red line for dehydrogenation into benzene). For Pt nanoparticles with a size of ~1–2 nm, there is no selectivity for hydrogenation and dehydrogenation. The product ratio is ~50% for each of them. However, the ratio of hydrogenation and dehydrogenation product increases with the increase of particle size. For nanoparticles with a size of ~7–8 nm, the selectivity is ~3:1 between hydrogenation and dehydrogenation. Definitely, the Pt nanocatalyst (7–8 nm) displays high catalytic selectivity for cyclohexene hydrogenation. In addition, measurements show the activation energy of cyclohexene dehydrogenation increases nearly linearly as Pt nanoparticle size is increased (green line of Fig. 18); however, the activation energy of hydrogenation (blue line) remains nearly constant as particle size is increased. The different dependences of activation energy on particle size indicate that hydrogenation and dehydrogenation may have different intermediates. These intermediates have different chemical affinity for surface catalytic sites determined by particle size. The dependence of catalytic

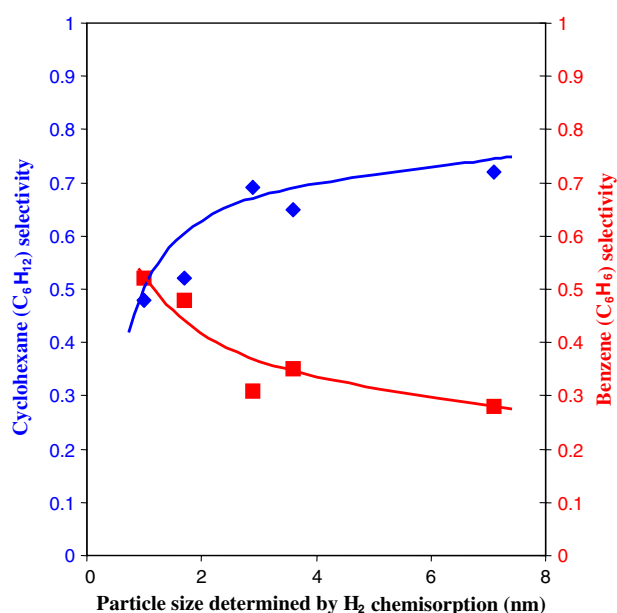


Fig. 17 Selectivity of cyclohexene hydrogenation to cyclohexane (blue line) and dehydrogenation to benzene (red line) as a function of Pt nanoparticle size measured by chemisorption of H₂. Reaction conditions are 10 Torr of C₆H₁₀ and 200 Torr of H₂ at 480 K

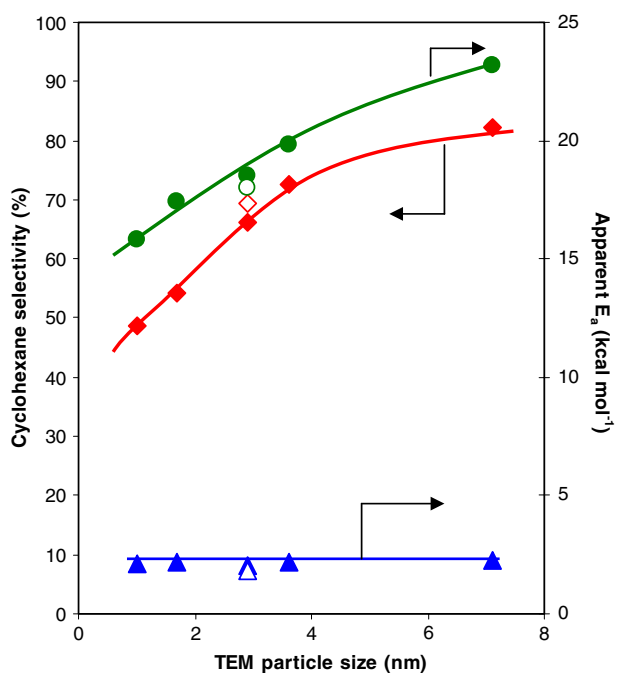


Fig. 18 Apparent activation energy of cyclohexene hydrogenation (blue line) and dehydrogenation (green line) and selectivity for hydrogenation into cyclohexane (red line) as a function of Pt nanoparticle size measured with TEM. Reaction condition is 10 Torr of C₆H₁₀ and 200 Torr of H₂ at 493 K

selectivity on size-determined structural factors is an important issue to study for understanding catalytic selectivity on metal nanoparticles. High-pressure scanning

tunnelling microscopy (STM) is probably the main technique addressing the structural and coupled electronic factors dominating catalytic selectivity.

4.3 Selective Site Blocking

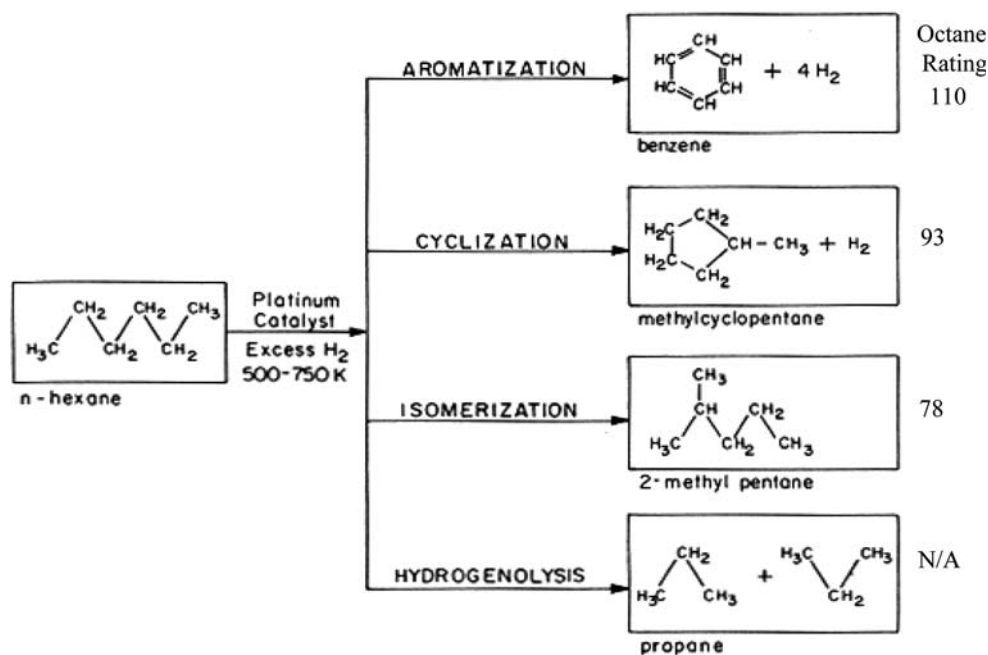
Selective site blocking is another strategy for the promotion of catalytic selectivity. As shown in Fig. 19, *n*-hexane has four conversion channels on Pt(111) at a temperature range of 500–750 K including aromatization into benzene, cyclization into metallylcyclopentane, isomerization into 2-methyl pentane, and hydrogenolysis into propane [1, 37]. Our studies demonstrated that selective site blocking for Pt(111) and Pt(100) surfaces via the formation of Pt–Au alloys on them can vary the selectivity for these reaction channels on Pt catalysts [38, 39]. The Pt–Au alloys were formed by the deposition of several monolayers of Au atoms from a Kundsens cell-type evaporation source onto Pt(111) or Pt(100) surface. Then, annealing at 1,070 K was carried out for thermal diffusion of the deposited Au atoms into Pt substrate and therefore forms a Pt–Au alloy on these single crystal surfaces.

Our studies show that the selectivity for multiple catalytic conversions of *n*-hexane on the Pt–Au alloy is significantly different from that on Pt(111) single crystal surface. Figure 20 presents the turnover frequency (TOF) of four conversions of *n*-hexane on this Pt–Au alloy catalyst as a function of Au surface coverage. The TOF of isomerization largely increases as a function of Au coverage on Pt(111) when Au coverage is smaller than ~ 0.25 ; it

doubles at coverage of ~ 0.25 ; then the TOF remains nearly constant in a coverage range of ~ 0.25 – 0.75 ; it rapidly drops at coverage larger than ~ 0.75 and then goes down to zero when Pt(111) is completely covered with Au atoms. The TOF of cyclization has a nearly linear decrease with the increase of Au coverage. For hydrogenolysis and aromatization, TOFs rapidly decrease at low coverage (≤ 0.50). Clearly, the Pt–Au alloy with certain Au coverage has significantly different TOFs for the four catalytic conversions. The TOF of each catalytic conversion as a function of Au coverage in Pt–Au alloys clearly demonstrated that the site blocking resulting from the formation of alloy is one promising strategy to promote selectivity of some specific catalytic reaction. For example, the selectivity of isomerization on Pt_{0.5}Au_{0.5} alloy is much larger than that on bare Pt(111) single crystal surface (Fig. 20).

The significant change in selectivity among isomerization, hydrogenolysis, and aromatization upon selective site blocking by Au atoms has been rationalized by ensemble effect [39]. In this argument, the hydrogenolysis and aromatization require a large ensemble of platinum atoms which is made of highly coordinated sites such as fourfold and threefold sites. However, as Au atoms substitutes for Pt atoms in the formation of Pt–Au alloy, the concentration of fourfold and threefold sites decreases more rapidly even though the Au coverage is very low. In addition, the rapid increase of isomerization rate at low coverage suggests that the isomerization occurs on small ensemble of Pt atoms made of lowly coordinated sites (twofold or one fold). A nearly constant high isomerization rate at an Au coverage of ~ 0.25 – 0.75 indicates that Au atoms may possibly

Fig. 19 Four conversion channels of *n*-hexane on Pt(111) single crystal surface at a temperature range of 500–750 K



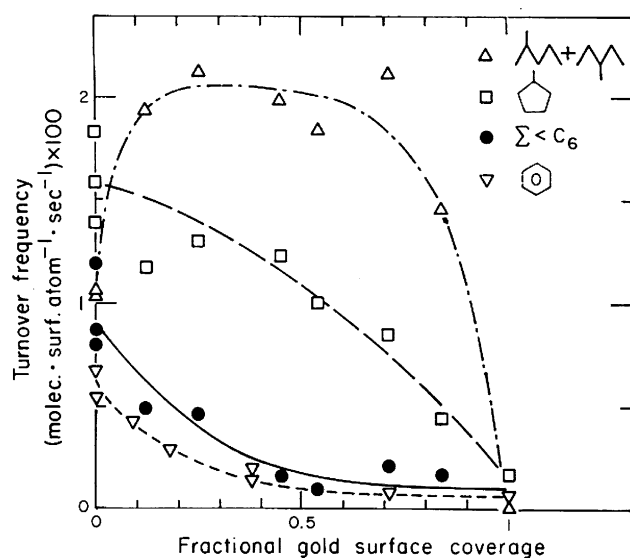


Fig. 20 Turnover frequencies of isomerization (Δ), cyclization (\square), hydrogenolysis (\bullet) and aromatization (∇) as a function of Au coverage in Pt–Au alloy formed on Pt(111) single crystal

directly particulate into the isomerization. The role of Au atoms in the catalytic sites of isomerization is possibly associated with electronic transfer between Au atoms and Pt atoms in alloy. This electron effect possibly varies the chemical binding of reactants and reactive intermediates on these sites and therefore modifies catalytic selectivity of these sites. Notably, for an Au coverage larger than ~ 0.75 , the rate of isomerization decreases very rapidly. It indicates that the catalytic sites of isomerization need at least one Pt atom. Figure 21 lists three catalytic sites for isomerization of *n*-hexane on Pt–Au alloy. Overall, the blocking of highly coordinated Pt sites by Au atoms in Pt–Au alloys grown on Pt(111) single crystal surface significantly decreases the rate of hydrogenolysis, aromatization, and cyclization since these conversions require large ensembles of Pt atoms. The

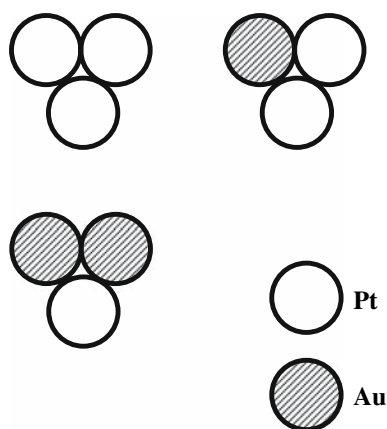


Fig. 21 Three categories of catalytic sites on Pt–Au alloy for isomerization of *n*-hexane

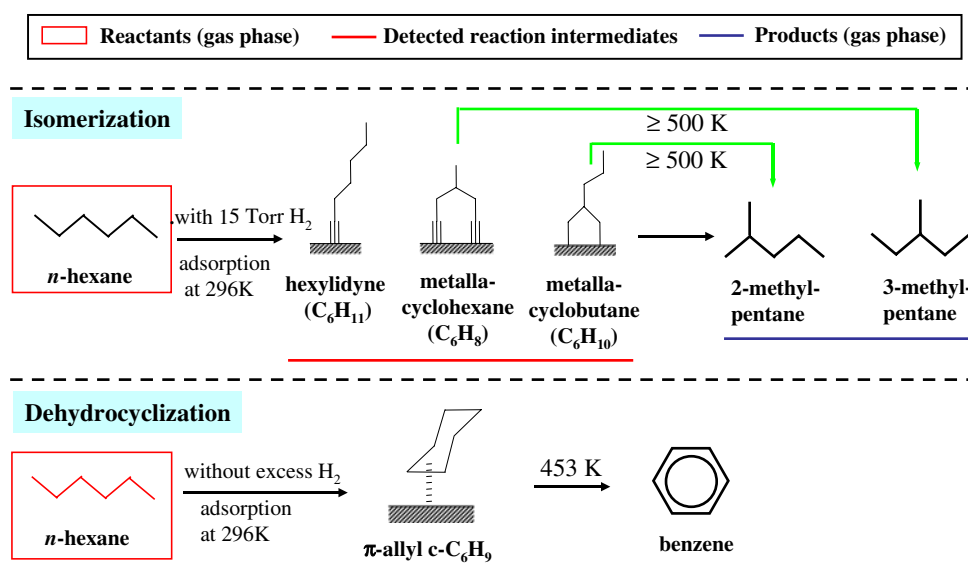
rate of isomerization, meanwhile, is largely increased as it needs small ensembles. Therefore, catalytic selectivity for isomerization is significantly promoted on Pt–Au alloy grown on Pt(111) with a Au coverage of ~ 0.5 – 0.75 . This ensemble effect and the contribution of electronic effect of Au atoms in the promotion of catalytic selectivity of hydrocarbon conversions can be further studied with a combination of scanning tunneling microscopy and scanning tunneling spectroscopy.

4.4 The Influence of Hydrogen Pressure on Catalytic Selectivity

n-hexane is the simplest alkane molecule, but it is large enough to carry out various skeletal rearrangement reactions involved in the hydrocarbon reforming process including dehydrogenation, isomerization, cyclization, and dehydrocyclization [40, 41]. Isomerization and dehydrocyclization of *n*-hexane are two of the most important reactions in naphtha reforming process as they produce the largest increase in octane number. Pt catalyst has the unique capability of hydrocarbon reforming. Importantly, the presence and absence of excess hydrogen gives different selectivity of reaction channels of *n*-hexane catalyzed by Pt(111) single crystal surface [37].

In the presence of excess hydrogen at 296 K, *n*-hexane is inactive on Pt(111). Upon heating to 453 K, *n*-hexane is partially dehydrogenated to form hexylidyne or metallacyclic species as shown in Fig. 22. When annealing to a temperature above 500 K, the two metallacyclic species isomerize into 2-methylpentane and 3-methylpentane. At a higher temperature, hydrogenolysis into propylene takes place. In the absence of excess hydrogen at 296 K, *n*-hexane dehydrogenates to form π -allyl $c\text{-C}_6\text{H}_9$. Upon heating to 453 K in the absence of excess hydrogen, the π -allyl $c\text{-C}_6\text{H}_9$ carries out irreversible dehydrogenation, forming benzene. Notably, during cooling cycles of π -allyl $c\text{-C}_6\text{H}_9$ species in the temperature range of 290–450 K, no metallacyclic or hexylidyne species can be detected. It indicates that dehydrocyclization of *n*-hexane to form π -allyl $c\text{-C}_6\text{H}_9$ in the absence of excess hydrogen and dehydrogenation of *n*-hexane to form a hexylidyne or metallacyclic species have different reaction pathways. π -allyl $c\text{-C}_6\text{H}_9$ is a reaction surface intermediate for dehydrocyclization of *n*-hexane to benzene. The dehydrocyclization of *n*-hexane to form benzene in the absence of excess hydrogen is carried out through a direct 1,6-ring closure rather than ring enhancement of methylcyclopentane. However, metallacyclic species and hexylidyne are reactive intermediates in the process of *n*-hexane isomerization through the methylcyclopentane formation in the presence of excess hydrogen (Fig. 22). The hydrogen effect on catalytic selectivity of

Fig. 22 Reaction mechanisms of isomerization and dehydrocyclization of *n*-hexane on Pt(111) single crystal surface in the presence and absence of excess hydrogen



n-hexane on Pt(111) was further confirmed by the increase of gas product ratio between benzene and methylcyclopentane with the decrease of hydrogen pressure. Thus, dehydrocyclization of *n*-hexane to benzene is dominant over isomerization of *n*-hexane in the absence of excess hydrogen. The difference in the catalytic selectivity from the presence or absence of excess hydrogen possibly results from an increase in the disorder of surface species and decrease in the surface coverage of the π -C₆H₉ intermediate due to the weakening of the hydrocarbon–Pt bond when excess hydrogen is present [37, 42].

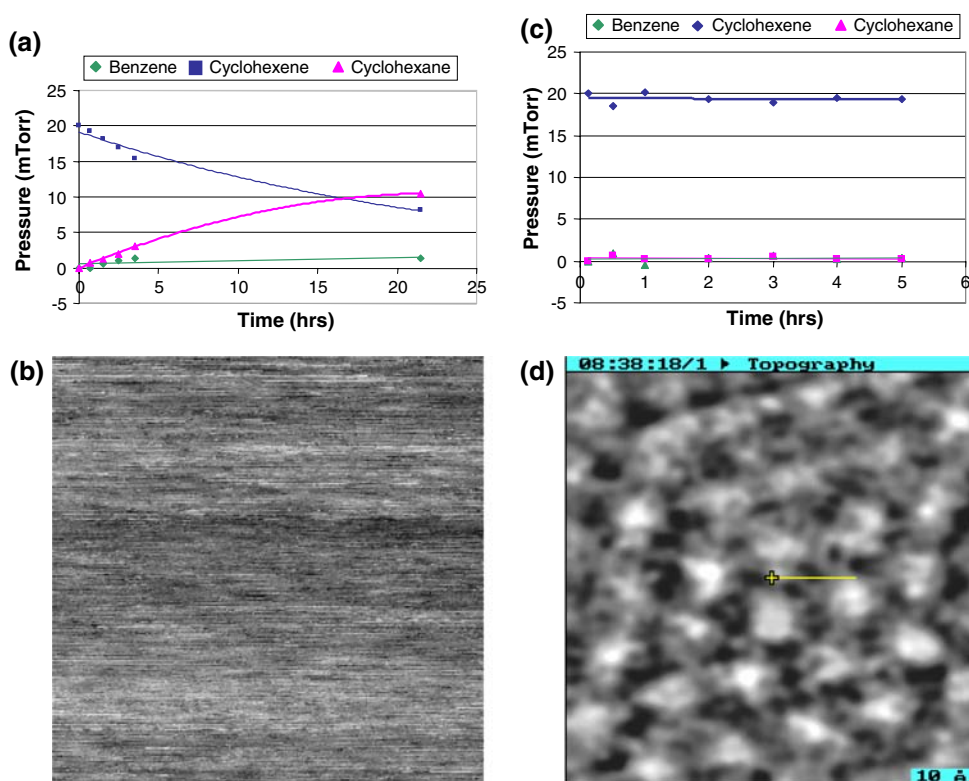
5 Challenges for the Near Future

The incorporation of nanoscience and nanotechnology into catalyst synthesis and catalysis study provides unique opportunity to address a number of unresolved issues in the studies of single crystal surface model catalyst and polycrystalline catalyst. Colloid chemistry controlled synthesis of nanoparticles and nanolithography fabrication of nanostructural materials produce high-technology catalysts with controllable size, size-distribution, and shape at nanoscale. High-pressure techniques including high-pressure STM, high-pressure sum frequency generation (SFG), and high-pressure X-ray photoelectron spectroscopy (XPS) are definitely the most important approaches to characterizing catalysts and studying catalytic reactions under high-pressure and high-temperature working environment of industrial catalysts. However, there is a long way until thorough elucidation of catalytic mechanisms of real catalysts. There are many challenges which involve the techniques of catalysis studies and the syntheses of nanocatalysts. For example, one challenge is how to use high-

pressure STM to visualize the movement of reactant molecules during catalytic reactions. This will definitely elucidate the role of molecular mobility in catalysis. Due to high mobility of reactant molecules and intermediate in cyclohexene hydrogenation and dehydrogenation there is no identifiable feature in the STM image of Pt(111) under a reaction condition of 200 mTorr H₂ and 20 mTorr cyclohexene. The occurrence of hydrogenation from cyclohexene into cyclohexane and dehydrogenation into benzene is evidenced by the increase of partial pressure of cyclohexane and benzene and the decrease of partial pressure of reactant cyclohexene (Fig. 23a). However, under the reaction condition of 200 mTorr H₂, 20 mTorr cyclohexene, and 5 mtorr CO, an obvious superstructure of chemisorbed CO molecules is formed on Pt(111) (Fig. 23c). The poison of CO for the catalytic site on Pt(111) is supported by the measurements of reactant and product. Clearly, the partial pressure of reactant remain constant and no product can be detected (Fig. 23d). Thus, the mobility of reactant molecules and intermediates is necessary for the occurrence of a catalytic reaction. Visualization of the mobility of these species is crucial for understanding catalytic mechanism at molecular level. For example, it can identify the catalytic sites of different products and thereby reaction selectivity of some required product can be enhanced by blocking other sites. To visualize molecular mobility and even identify intermediates, STM needs a faster scan speed than molecular movement at room temperature or even high temperature. This is definitely a challenge at the technological side of catalytic studies.

From the side of materials synthesis, the Langmuir–Blodgett monolayer of 3-D nanoparticles synthesized via colloid chemistry is an excellent model catalyst for

Fig. 23 (a) Evolution of cyclohexane and benzene on Pt(111) at 25 °C, 200 mTorr H₂, 20 mTorr cyclohexene. (b) 75 Å × 75 Å image of catalytically active Pt(111) at 25 °C, 200 mTorr H₂ and 20 mTorr cyclohexene added. (c) 70 Å × 70 Å image of CO poisoned Pt(111) at 25 °C. (d) Evolution of cyclohexane and benzene on Pt(111), 200 mTorr H₂, 20 mTorr cyclohexene, 5 mTorr CO at 25 °C. (e) 70 Å × 70 Å image of CO poisoned Pt(111) at 25 °C, 200 mTorr H₂, 20 mTorr cyclohexene, and 5 mTorr CO added



nanoscale catalytic studies by using high pressure STM because (1) the controllable size and shape of nanoparticles offers opportunity for revealing size- and crystallographic face-dependent catalysis mechanism, (2) its controllable inter-particle distance provides convenience for studying molecular mobility and reaction pathway, and (3) the nanoparticle-oxide substrate interface can be used to address the functions of interface and catalyst support. However, the challenge of this model catalyst is the removal of polymeric capping agents bound to nanoparticles for structural and electronic characterization at atomic level. It is also a challenge for 3-D high technology catalysts assembled in mesoporous support such as SBA-15.

Acknowledgement This work was supported by the Director, Office of Science, Office of Advanced Scientific Computing Research, Office of Basic Energy Sciences, Chemical Sciences, Geosciences, and Biosciences Divisions and the Materials Sciences and Engineering Divisions, of the U.S. Department of Energy under Contract No. DE-AC02-05CH11231.

References

- Somorjai GA (1994) Introduction to surface chemistry and catalysis. John Wiley & Sons, New York
- Yan XM, Kwon S, Contreras AM, Bokor J, Somorjai GA (2005) Nano Lett 5:745
- Yan XM, Contreras AM, Koebel MM, Liddle JA, Somorjai GA (2005) Nano Lett 5:1129
- Kwon S, Yan XM, Contreras AM, Liddle JA, Somorjai GA, Bokor J (2005) Nano Lett 5:2557
- Jacobs PW, Ribeiro FH, Somorjai GA, Wind SJ (1996) Catal Lett 37:131
- Jacobs PW, Wind SJ, Ribeiro FH, Somorjai GA (1997) Surf Sci 372:L249
- Choi YK, Zhu J, Grunes J, Bokor J, Somorjai GA (2003) J Phys Chem B 107:3340
- Zhu J, Somorjai GA (2001) Nano Lett 1:8
- Konya Z, Puentes VF, Kiricsi I, Zhu J, Alivisatos AP, Somorjai GA (2002) Nano Lett 2:907
- Hoefelmeyer JD, Niesz K, Somorjai GA, Tilley TD (2005) Nano Lett 5:435
- Song H, Rioux RM, Hoefelmeyer JD, Komor R, Niesz K, Grass M, Yang PD, Somorjai GA (2006) J Am Chem Soc 128:3027
- Rioux RD, Song H, Hoefelmeyer JD, Yang P, Somorjai GA (2005) J Phys Chem B 109:2192
- Grunes J (2004) Ph.D. Thesis, University of California, Berkeley
- Tsirlin T, Zhu J, Grunes J, Somorjai GA (2002) Top Catal 19:165
- Eppler AS, Zhu J, Anderson EA, Somorjai GA (2000) Top Catal 13:33
- Choi YK, Zhu J, Grunes J, Bokor J, Somorjai GA (2003) J Phys Chem B 107:3340
- Teranishi T, Hosoe M, Tanaka T, Miyake M (1999) J Phys Chem B 103:3818
- Wang Y, Ren J, Deng K, Gui L, Tang Y (2000) Chem Mater 12:1622
- Ahmadi TS, Wang ZL, Green TC, Henglein A, El-Sayed MA (1996) Science 272:1924
- Somorjai GA, Rupprechter G (1999) J Phys Chem 103:1623
- Levin ME, Salmeron M, Bell AT, Somorjai GA (1987) J Catal 106:401
- Tauster SJ (1987) Acc Chem Res 20:389
- Bartholomew CH, Pannell RB, Butler JL (1980) J Catal 65:335

24. Boffa A, Lin C, Bell AT, Somorjai GA (1994) *J Catal* 149:149
25. Somorjai GA (2005) *Catal Lett* 101:1
26. Ji X, Zuppero A, Gidwani JM, Somorjai GA (2005) *J Am Chem Soc* 127:5792
27. Park JY, Somorjai GA (2006) *J Vac Sci Technol B* 24:1967
28. Park JY, Somorjai GA (2006) *Chem Phys Chem* 7:1409
29. Schwab GM, Darleth H (1966) *J Phys Chem Beue Folge* 50:191
30. Schwab GM, Darleth H (1967) *J Phys Chem Neue Folge* 53:1
31. Solymosi F (1967) *Catal Rev* 1:233
32. Langenbeck W, Dreyer H, Fuhrman H (1962) *J Anorg Chem* 314:179
33. Schwab GM, Putzar R (1962) *J Phys Chem (Frankfurt)* 31:179
34. Contreras AM, Grunes J, Yan XM, Liddle A, Somorjai GA (2005) *Catal Lett* 100:115
35. Grunes J, Zhu J, Yang M, Somorjai GA (2003) *Catal Lett* 86:157
36. Haruta M (1997) *Catal Today* 36:153
37. Yang M, Somorjai GA (2004) *J Am Chem Soc* 126:7698
38. Yeates RC, Somorjai GA (1987) *J Catal* 103:208
39. Sachtler JWA, Somorjai GA (1983) *J Catal* 81:77
40. Zaera F, Godbey D, Somorjai GA (1986) *J Catal* 101:73
41. Davis SM, Zaera F, Somorjai GA (1984) *J Catal* 85:206
42. Yang MC, Chou KC, Somorjai GA (2004) *J Phys Chem B* 108:14766